Non Fickian flux for advection–dispersion with immobile periods

Non Fickian flux for advection–dispersion with immobile periods

Boris Maryshev[1]**, Maminirina Joelson**[2]**, Dimitri Lyubimov**[3]**, Tatiana Lyubimova**[1] **and Marie-Christine Néel**[2]

[1] ICMM, Institute of Continuous Media Mechanics, Russian Academy of Science, Ural Branch, 1 Koroleva street, 614013 Perm, Russia
[2] Université d'Avignon et des Pays de Vaucluse, UMR 1114 EMMAH, F-84018 Avignon, France
[3] Department of Theoretical Physics, Perm State University, 15 Bukireva street, 614990 Perm, Russia

E-mail: bmaryshev@mail.ru, maminirina.joelson@univ-avignon.fr, lyubimov@psu.ru, lyubimova@psu.ru and mcneel@avignon.inra.fr

Abstract

The fractal mobile–immobile model (MIM) is intermediate between advection–dispersion (ADE) and fractal Fokker–Planck (FFKPE) equations. It involves two time derivatives, whose orders are 1 and γ (between 0 and 1) on the left-hand side, whereas all mentioned equations have identical right-hand sides. The fractal MIM model accounts for non-Fickian effects that occur when tracers spread in media because of through-flow, and can get trapped by immobile sites. The solid matrix of a porous material may contain such sites, so that non-Fickian spread is actually observed. Within the context of the fractal MIM model, we present a mapping that allows the computation of fluxes on the basis of the density of spreading particles. The mapping behaves as Fickian flux at early times, and tends to a fractional derivative at late times. By means of this mapping, we recast the fractal MIM model into conservative form, which is suitable to deal with sources and bounded domains. Mathematical proofs are illustrated by comparing the discretized fractal p.d.e. with Monte Carlo simulations.

PACS numbers: 05.60.−k, 46.65.+g, 05.40.Fb, 02.60.Nm

1. Introduction

A pioneering example, devoted to charge carriers in heterogeneous media [1, 2], indicated that mass transport is not always appropriately described by Fick's law. Indeed, in many situations, the spread of a cloud of walkers (as different as passive contaminant particles, living organisms

or financial values) is found to grow nonlinearly with time. Such features have been often described in terms of partial differential equations (p.d.e) involving derivatives of non-integer order with respect to (w.r.t) space or time [3–6], whereas nonlinear models also are currently being investigated [7].

The successes of the classical advection–dispersion equation (ADE), which arises from coupling Fick's law for fluxes with the mass conservation principle, are not only supported by the fitting of many experimental data. Indeed, the ADE also represents the hydrodynamic limit of a class of small-scale models, where the motion of independent walkers is composed of accumulating Gaussian jumps, and the theoretical upscaling [8] has been substantiated by actual experiments showing walker trajectories, as recalled in [9]. Fractional p.d.e. are more general (they can indeed be viewed as an extension of the ADE) and were also proved to be hydrodynamic limits of stochastic models [5, 6] accounting for heavy-tailed jumps and/or waiting times. Hence, they represent a preferential tool toward the description of experimental data displaying non-Fickian features. Rigorous proofs directly connecting macroscopic fractional models to small-scale scenarios for individual walkers [5, 10], lie in the assumption that trajectories and time clocks sum up independent identically distributed random variables, thus falling into the field of center limit theorems [11–14]. Directly checking such hypotheses is far from trivial, nevertheless the asymptotics of the probability laws, common to such random variables, imposes the order of the derivatives appearing in the corresponding macroscopic models. Hence, mastering that models should help in understanding small-scale experiments, where capturing the behavior of the distribution tails is precisely not easy at all. Of course, there are many situations where independence of repeated events does not hold: in this case, both ADE and fractional generalizations may be inappropriate, and other approaches are needed [7].

Here we focus on dispersion phenomena that compare at least qualitatively with small-scale motions where Gaussian jumps and advection are in competition with random sticking events, temporarily shielding tracers from the influence of the mean flow stream. At the macroscopic level, such situations are mirrored into heavy-tailed breakthrough curves (BTC) decreasing at some power of time, negative but larger than -2. Similar behavior has been observed, e.g. in the context of contaminant transport in specific kinds of porous media where trapping sites and a tendency to sticking have been reported [15]. Besides the spreading of passive tracers in unsaturated porous media [16, 17], we have in mind qualitative observations of colloids sorbing at some sites in the solid porous matrix [18].

A class of p.d.e. called the 'fractal Mobile–Immobile Medium' model [19] is apparently very promising for such situations. It is a variant of the standard MIM model [20], where tracers are assumed to have two phases, mobile and immobile, and mass exchanges between the two obey first-order kinetics. The 'fractal' version is better suited to capture BTC with heavy-tailed trailing edges. Up to the presence of a first-order time derivative, the fractal model is akin to the better known fractional Fokker–Planck equation (FFPE) [21, 22], whose long time asymptotics shows similar features. All these fractional p.d.e.'s represent hydrodynamic limits of stochastic processes, assuming that independent particles accumulate random independent Gaussian jumps separated by time intervals. Numerical experiments by [15] show that a combination of immobilization intervals (whose durations obey a heavy-tailed distribution) and constant time periods devoted to advection and dispersion, corresponds to the fractal MIM model. In order to facilitate the processing of data issued from laboratory experiments where the most easily accessed quantity is the out coming flux, we focus on finding the proper expression for Fick's law to be used when the underlying model is the fractal MIM. This effort is motivated by the prominent role of boundary conditions, often involving fluxes, in laboratory experiments, which necessarily take place in bounded domains, such as finite

length columns. The expression for fluxes will be shown to result in a conservative evolution equation, better suited than the fractal MIM model itself to deal with sources of tracer [23], hence more general. Last but not least, conservative schemes (directly connected with fluxes in the spirit of finite volume methods) frequently allow the use of clever numerical methods.

After recalling equations used for mass transport with heavy tails, in section 2 we propose an expression for fluxes, and recast the fractal MIM model into a conservative form. In section 3 we show that the proposed model indeed rules the density of stochastic transport processes involving randomly distributed immobile events intervening between mobile periods, under specific conditions. Numerical solutions, compared with Monte Carlo simulations, will illustrate the results of sections 2 and 3, and emphasize that the conservative form is indeed appropriate for problems involving a forcing term.

2. Fick's law with long-term memory

Many experimental data involving transport in the environment, or in laboratory columns filled with porous material, show rapidly increasing BTC, followed by a trailing edge whose prominence and duration vary, depending on the material and on the flow conditions [15–17, 24, 25]. A huge collection of field- as well as laboratory-scale experiments supports such non-Fickian effects. They are not compatible with the ADE (where fluxes obey Fick's law), and the original MIM model represents an important progress in view of such situations [20]. Nevertheless, very marked heavy-tailed trailing edges, observed especially in the case of passive tracers in unsaturated conditions [16, 17], and also of certain bacteria in saturated sand [18], remain out of reach. The fractal variant is more appropriate to describe such data, and we will see that it can be put into a conservative form.

2.1. Fractal MIM model

The original MIM model builds upon the fact that, in many natural porous media, tracers may temporarily be stopped at immobile sites, which may be disseminated in the solid matrix. The model was indeed developed by hydrologists, often facing situations where only the 'mobile' phase is accessible to field measurements. The simplest form of the model assumes first-order kinetics for exchanges between mobile and immobile phases. Solving the kinetic equation ruling the immobile concentration, allows the determination of the total density of tracer, in the form of a single equation. The equation appears as a modified ADE, involving a convolution with an exponential kernel, besides the regular time derivative on the left-hand side. In the limit of small relaxation times, we thus obtain a constant factor larger than 1, in front of that derivative (the well-known retardation factor). Processing along the same lines, it can be shown that power-like kernels yield the fractal version [15, 19, 26]

$$\partial_t C(x, t) + \lambda \partial_t^\gamma C(x, t) = L C(x, t), \tag{1}$$

for the total density of tracer (accounting for mobile and immobile phase together). With $\lambda \neq 0$, equation (1) captures the above-mentioned non-Fickian effects with heavy tails. Often, these features are referred to as 'memory effects'; indeed, the presence of power laws implies that the past history of each particle is forgotten very slowly in time. The model reduces to the classical ADE when $\lambda = 0$, and the original MIM model corresponds to (1) with $\gamma = 1$. In the linear mapping $L = K\Delta - v \cdot \nabla$, we have the Laplacian operator Δ and the gradient ∇, whereas K and v represent diffusivity and mean flow velocity. On the left-hand side of (1), we have the Caputo fractional derivative ∂_t^γ, whose definition and basic properties are recalled in appendix A. Equation (1) was introduced by [19], then used by [15] in order to represent field data for the evolution of a dissolved tracer in heterogeneous aquifers.

Equation (1), and also

$$\partial_t^\gamma C(x,t) = LC(x,t), \tag{2}$$

more widely used (with γ in $]0,1]$) are particular cases of the more general time-fractional diffusion equation of distributed order [32, 33]

$$\left(\int_0^1 w(\mathrm{d}\beta)\partial_t^\beta\right) C(x,t) = \left(\int_0^1 w(\mathrm{d}\beta)I_{0,+}^{1-\beta}\right)\partial_t C(x,t) = LC(x,t),$$

with $w = \delta_0 + \lambda\delta_\gamma$ for (1) and $w = \delta_\gamma$ for (2). Here δ_a represents the Dirac measure concentrated on point a. Equation (2) [9, 22] is equivalent to $\partial_t C(x,t) = D_{0,+}^{1-\gamma} LC(x,t)$, which may also be written as [34]

$$\partial_t C(x,t) = LD_{0,+}^{1-\gamma} C(x,t), \tag{3}$$

where we have the Riemann–Liouville derivative $D_{0,+}^{1-\gamma}$, whose definition is recalled in appendix A. Equations (2) and (3) are equivalent when K and v are time independent. Nevertheless, inhomogeneous problems issued from (2) and (3) by adding some forcing $r(x,t)$ on the right-hand side are not equivalent [23]. Equation (2) has been applied to the fitting of many BTC, obtained at the exit of porous columns (with constant flow), though it hardly captures both early and late time behavior [16, 17]. Addressing fluxes of particles spreading according to equation (1) will help us seeing that the fractal MIM model describes heavy-tailed BTC as well as FFPE, without missing Fickian early behavior.

2.2. Conservative form for (1)

The ADE corresponds to mass conservation principle, combined with classical Fick's law. This latter states that the flux $F(x,t)$ of spreading matter through x at instant t is [35, 36]

$$F(x,t) = -K\nabla C(x,t) + C(x,t)v.$$

If (2) holds, instead we have

$$F(x,t) = -K\nabla D_{0,+}^{1-\gamma} C(x,t) + D_{0,+}^{1-\gamma} C(x,t)v.$$

According to the definitions of fractional integrals and derivatives, recalled in appendix A, equation (1) corresponds exactly to $\left(\mathrm{Id} + \lambda I_{0,+}^{1-\gamma}\right)\partial_t C(x,t) = LC(x,t)$, where Id denotes identity. Moreover, the mapping $\mathrm{Id} + \lambda I_{0,+}^{1-\gamma}$, equivalent to multiplication by $1 + \lambda s^{\gamma-1}$ in Laplace variables (see the remark of appendix A), is proved in appendix B to have an inverse operator which we call $\left(\mathrm{Id} + \lambda I_{0,+}^{1-\gamma}\right)^{-1}$. Therefore, equation (1) is equivalent to mass conservation law

$$\partial_t C(x,t) = -\nabla \cdot F(x,t) \tag{4}$$

combined with a flux

$$F(x,t) = -K\nabla\left(\mathrm{Id} + \lambda I_{0,+}^{1-\gamma}\right)^{-1} C(x,t) + \left(\mathrm{Id} + \lambda I_{0,+}^{1-\gamma}\right)^{-1} C(x,t)v. \tag{5}$$

Appendix B also shows that similar expressions for fluxes correspond to more general fractional equations of distributed order. In section 5, we will see that inserting a source delivering particles according to rate $r(x,t)$ results in adding the forcing term $r(x,t)$ on the right-hand side of (4).
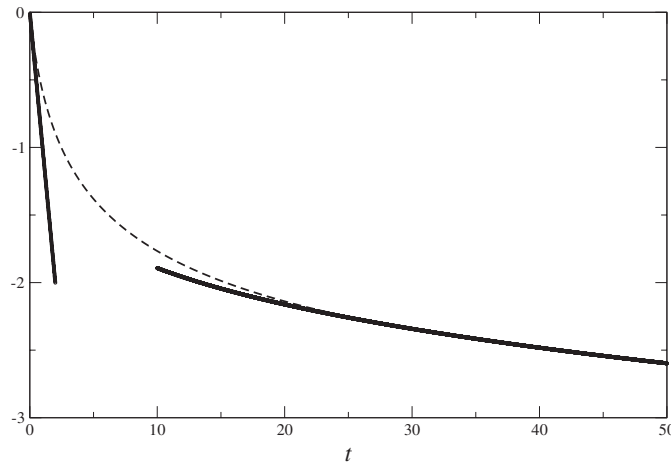
Figure 1. Variations of $(\mathrm{Id} + \lambda I_{0,+}^{1-\gamma})^{-1} f(t)$, compared with $f(t)$ itself and $\lambda^{-1} D_{0,+}^{1-\gamma} f(t)$ for small, respectively large, values of t. We took $f(t) = -t$, $\lambda = 1$ and $\gamma = 0.75$. The dashed curve stands for $(\mathrm{Id} + \lambda I_{0,+}^{1-\gamma})^{-1} f(t)$, thick lines at the left and at the right correspond to $f(t)$ and $\lambda^{-1} D_{0,+}^{1-\gamma} f(t)$, respectively.

2.3. Early and late time behavior for fluxes

When t is small, $\left(\mathrm{Id} + \lambda I_{0,+}^{1-\gamma}\right)^{-1} f(t)$ is very close to $f(t)$, since $I_{0,+}^{1-\gamma}$ is a small mapping of $L^p[0, T]$ (cf appendix B). When t is large, in contrast $\left(\mathrm{Id} + \lambda I_{0,+}^{1-\gamma}\right)^{-1} f(t)$ is approximately $\frac{1}{\lambda} D_{0,+}^{1-\gamma} f(t)$, as we can see from appendix C: we recover the flux corresponding to (2) or (3). Hence (1) and (5) bridge between Fickian fluxes at early times and non-Gaussian behavior at late times, due to the release of previously trapped particles. In section 4, we present specific methods allowing us to compute the mapping $\left(\mathrm{Id} + \lambda I_{0,+}^{1-\gamma}\right)^{-1}$. An example showing early, intermediate and late time behavior, is represented in figure 1.

Equation (3) is the hydrodynamic limit of a stochastic scenario, involving Gaussian random jumps performed during power-law distributed time series [22]. We will see that equation (1) and equivalent form (4) also represent the macroscopic version of a small-scale model for dispersion, involving immobile time periods for the walkers.

3. Small-scale model for (1)

The idea that particles of tracer may undergo periods of immobilization corresponds to the letter I in the 'MIM' acronym. Equations such as (3) were shown to rule the density of some process $X(t)$ subordinated to the hitting time process of a stable subordinator, provided the density of $X(t)$ satisfies the Fokker–Planck equation with force field v [22]. Following indications of [15], we will see that equation (1) also describes Brownian motion with drift (possibly modified in view of boundary conditions), intermixed with immobile random periods.

3.1. Fickian advection–dispersion

With $\lambda = 0$, (1) is the standard ADE, which rules the evolution of the propagator $q(x, t)$ of a Brownian motion, with a drift representing advection speed v. We restrict our attention to the

one-dimensional case, and consider space domains which may be either infinite, or limited by 'natural' boundary conditions as follows. Inserting an absorbing limit

$$q(x_1, t) = 0 \tag{6}$$

at abscissa x_1 means that particles arriving there are killed. On the other hand, inserting a zero-flux condition

$$-K\partial_x q(x_0, t) + vq(x_0, t) = 0 \tag{7}$$

means that particles bounce back when hitting an elastic wall, located at x_0.

In order to see later that the fractional derivative ∂_t^γ appears in (1) when we impose random sticking times, as in [15], we will consider a random process $X(t)$ whose probability density function (p.d.f.) $q(x, t)$ satisfies

$$\partial_t q(x, t) = \left(K\partial_{x^2}^2 - v\partial_x\right)q(x, t) \tag{8}$$

in the domain $]x_0, x_1[$, which may be infinite or bounded, and associated with boundary conditions such as (6)–(7). Moreover, $X(t)$ is assumed start from the initial condition

$$q(x, 0) = \varphi(x). \tag{9}$$

x_1, which may represent the inlet and the outlet of a device subjected to constant through flow of speed v. Process $X(t)$ can be thought of as being the limit, when dt tends to zero, of a random walk performed by independent particles accumulating independent jumps, distributed as $\sqrt{2K\,dt}N$, with N a Gaussian normalized and centered random variable. Moreover, during time intervals of duration dt separating the jumps, particles move at velocity v. In an infinite domain, the location of a tagged particle at time $\tau = n\,dt$ is distributed as

$$X_{dt}(\tau) = n^{1/2}\sqrt{2K\,dt}N + v\tau = \sqrt{2K\tau}N + v\tau,$$

which only depends on τ. The p.d.f. of process $X_{dt}(\tau)$ tends to that of $X(\tau)$ when dt tends to zero. In a bounded domain, limited by the zero-flux boundary condition (7), $X_{dt}(\tau)$ does not describe the location of a tagged walker, but gives the distance, covered along trajectories. Nevertheless, the particle density tends to the solution q of (6)–(9), when dt tends to zero [36].

3.2. Advection–dispersion with sticking

We now modify the random walk: just after each period of duration dt, we insert independent random sticking times, distributed as d$t^{1/\gamma}W$, the random variable W following a stable Lévy law of exponent $0 < \gamma < 1$, concentrated on R^+. The p.d.f. $u_{\gamma,\lambda}$ of W has Laplace transform $e^{-\lambda s^\gamma}$ [15].

Trajectories are not modified, but time schedules are different. Mobile and immobile periods have different time scales, with very different long-time behavior due to the infinite mean of W. Because it is a sum of independent identically distributed stable random variables, the total sticking time corresponding to n mobile events of overall duration $n\,dt$ is, in turn, a stable random variable [11], of density $\frac{1}{n^{1/\gamma}} \times \frac{1}{dt^{1/\gamma}} u_{\gamma,\lambda}\left(\frac{\cdot}{n^{1/\gamma}\,dt^{1/\gamma}}\right)$. Hence, when the mobile (or operational) time is τ, the total sticking time a tagged particle spent in traps, is given by the γ-stable strictly increasing Lévy motion $U(\tau)$ whose p.d.f. is $\frac{1}{\tau^{1/\gamma}} u_{\gamma,\lambda}\left(\frac{y}{\tau^{1/\gamma}}\right)$. The clock time is $U(\tau) + \tau$ instead of τ, and the delay $U(\tau)$ may be significant, since W has infinite mean. The inverse process

$$Z_t = \inf\{\tau/U(\tau) + \tau > t\}$$

represents the operational time at clock time t (the real physical time).

Hence, following the lines of [22] (where time intervals between jumps correspond to $U(\tau)$ instead of $U(\tau) + \tau$), we address the p.d.f. $p(x, t)$ of process $Y(t) = X(Z_t)$, computing

the location at instant t of a particle performing the above Brownian motion $X(t)$, subordinated to Z_t. We will prove the following theorem.

Theorem 1. *Let $X(t)$ be a stochastic process whose p.d.f. $q(x, t)$ solves (8) in $]x_0, x_1[$, and satisfies initial and boundary conditions (9) and (6)–(7). Then, if U is a γ-stable strictly increasing Lévy motion whose p.d.f. has Laplace transform $e^{-\lambda\tau s^\gamma}$ while Z_t denotes the inverse process of $U(\tau) + \tau$, the p.d.f. $p(x, t)$ of the subordinated process $Y(t) = X(Z_t)$ solves (1) and satisfies (9) and (6)–(7).*

3.3. Proof of the theorem

Since $X(t')$ and Z_t are independent processes, with parameters t' and t, the p.d.f. $p(x, t)$ of the subordinated process $Y(t)$ is given by [22, 37, 38]

$$p(x, t) = \int_0^\infty q(x, \tau)g(\tau, t)\,d\tau,$$

where $g(\tau, t)$ is the p.d.f of Z_t. Hence, the Laplace transform $\tilde{p}(x, s)$ of $p(x, t)$ is equal to

$$\tilde{p}(x, s) = \int_0^{+\infty} q(x, t')\tilde{g}(t', s)\,dt'. \tag{10}$$

Now, let us compute g and $\tilde{g}$. Since process $U(\tau) + \tau$ is strictly increasing and right continuous [10], we have $P\{U(\tau) + \tau > t\} = P\{Z_t < \tau\}$, from which we deduce

$$P\{U(\tau) + \tau > t\} = 1 - \int_0^{\frac{t-\tau}{\tau^{1/\gamma}}} u_{\gamma,\lambda}(z)\,dz,$$

hence

$$g(\tau, t) = \partial_\tau P\{U(\tau) + \tau > t\} = \left[\frac{t}{\gamma\tau^{1+1/\gamma}} + (1 - 1/\gamma)\frac{1}{\tau^{1/\gamma}}\right]u_{\gamma,\lambda}\left(\frac{t-\tau}{\tau^{1/\gamma}}\right).$$

Noting that the Laplace transform of $\frac{t}{\gamma\tau^{1+1/\gamma}}u_{\gamma,\lambda}\left(\frac{t-\tau}{\tau^{1/\gamma}}\right)$ is

$$\int_0^{+\infty} e^{-st}\frac{t}{\gamma\tau^{1+1/\gamma}}u_{\gamma,\lambda}\left(\frac{t-\tau}{\tau^{1/\gamma}}\right)dt = -\frac{1}{\gamma\tau}\partial_s\int_0^{+\infty} e^{-st}\frac{1}{\tau^{1/\gamma}}u_{\gamma,\lambda}\left(\frac{t-\tau}{\tau^{1/\gamma}}\right)dt,$$

since also the Laplace transform of $u_{\gamma,\lambda}$ is $e^{-\lambda s^\gamma}$, for $g(\tau, t)$ we have

$$\tilde{g}(\tau, s) = -\frac{1}{\gamma\tau}\partial_s e^{-\lambda\tau s^\gamma - s\tau} + \left(1 - \frac{1}{\gamma}\right)e^{-\lambda\tau s^\gamma - s\tau} = (\lambda s^{\gamma-1} + 1)e^{-\lambda\tau s^\gamma - s\tau}.$$

This implies $\frac{\tilde{p}(x,s)}{\lambda s^{\gamma-1}+1} = \tilde{q}(x, s + \lambda s^\gamma)$, due to (10). Recalling that $\tilde{q}(x, s)$ satisfies $s\tilde{q}(x, s) - \varphi(x) = L\tilde{q}(x, s)$ for any positive valued s, and noting that the mapping $s \mapsto s + \lambda s^\gamma$ in one to one in $]0, +\infty[$, we also have

$$(s + \lambda s^\gamma)\tilde{q}(x, s + \lambda s^\gamma) - \varphi(x) = L\tilde{q}(x, s + \lambda s^\gamma)$$

in $]x_0, x_1[$, hence

$$(s + \lambda s^\gamma)\frac{\tilde{p}(x, s)}{1 + \lambda s^{\gamma-1}} - \varphi(x) = L\frac{\tilde{p}(x, s)}{1 + \lambda s^{\gamma-1}}. \tag{11}$$

Now, let $C(x, t)$ solve (1) in $]x_0, x_1[$, and satisfy the boundary conditions (6), (7) and the initial data (9) we have

$$(s + \lambda s^\gamma)\tilde{C}(x, s) - (1 + \lambda s^{\gamma-1})\varphi(x) = L\tilde{C}(x, s).$$

Hence, $F(x, s) = \tilde{p}(x, s) - \tilde{C}(x, s)$ solves $(s + \lambda s^\gamma)F(x, s) = LF(x, s)$ in $]x_0, x_1[$ with (6), (7), and is therefore equal to zero in $]x_0, x_1[$, which proves the claim.

   Random walks provide discrete approximations to process $Y(t)$, hence to solutions to (1). Comparing histograms against numerical simulations of (1) or (4) will yield an alternative proof of the relationship between (1) or (4) and process $Y(t)$, and of the relevance of (5) for fluxes.

4. Numerical illustration

Accurate numerical schemes, based upon discrete approximations to Caputo and Riemann–Liouville derivatives, are available for equations (2), (3) [40, 41]. They adapt to equations (1) and (4), whereas computing fluxes need a discrete approximation to the inverse of $(\mathrm{Id} + \lambda I_{0,+}^{1-\gamma})$. Inverting this mapping yields an alternative method discretizing those equations, which compares satisfactorily with the above mentioned more classical schemes, and will allow us to prove numerically that equations (1)–(4) and (5) describe advection–dispersion with sticking.

4.1. Computing the inverse of $(\mathrm{Id} + \lambda I_{0,+}^{1-\gamma})$

We will see that discretizing $(\mathrm{Id} + \lambda I_{0,+}^{1-\gamma})$ yields an algebraic system, whose inverse approximates $(\mathrm{Id} + \lambda I_{0,+}^{1-\gamma})^{-1}$.

For g a given function, defined on R^+, $(\mathrm{Id} + \lambda I_{0,+}^{1-\gamma})^{-1} g$ is f, such that $g(t') = (\mathrm{Id} + \lambda I_{0,+}^{1-\gamma}) f(t')$ in $[0, t]$, which we discretize according to $t = n\Delta t$. Functions g and f are represented by the vectors $\mathbf{G}^{(n)}$ and $\mathbf{F}^{(n)}$, whose coordinates are the $g(j\Delta t)$ and $f(j\Delta t)$, denoted by $g^{(j)}$ and $f^{(j)}$, with $0 \leqslant j \leqslant n$. Approximating $I_{0,+}^{1-\gamma} f(t')$ (for $0 \leqslant t' \leqslant t$) by $\Sigma_{i=0}^{n'} w_i f^{(n'-i)}$ with $0 \leqslant n' \leqslant n$, yields $\mathbf{W}^{(n)}\mathbf{F}^{(n)} = \mathbf{G}^{(n)}$, where $\mathbf{W}^{(n)} = (W_{i,j}^{(n)})$ is the lower triangular array of dimension $(n+1) \times (n+1)$, of elements $W_{i,i}^{(n)} = 1 + \lambda w_0$, $W_{i,i-j}^{(n)} = \lambda w_j$ for $0 < j$ and $W_{i,i+j}^{(n)} = 0$, which we have to invert. Because of the structure of $\mathbf{W}^{(n)}$, the inverse is another lower triangular array $\mathbf{B}^{(n)} = (B_{i,j}^{(n)})$, of the form of $B_{i,i}^{(n)} = b_0^{(n)}$, $B_{i,i-j}^{(n)} = b_j^{(n)}$ for $0 \leqslant j \leqslant i \leqslant n$ and $B_{i,i+j}^{(n)} = 0$ for $0 < j$, with $b_i^{(n)}$ filling the diagonal of rank i. And arrays $\mathbf{B}^{(n)}$ can be stored in a vector form, which is very convenient to save computer's memory. Hence the inverse $(\mathrm{Id} + \lambda I_{0,+}^{1-\gamma})^{-1}$ is of the form $\Sigma_{i=0}^{n} b_i^{(n)} f^{(n-i)}$.

Not surprisingly, the quality of the resulting scheme for $(\mathrm{Id} + \lambda I_{0,+}^{1-\gamma})^{-1}$ depends on the accuracy of the approximation $\Sigma_{i=0}^{n} w_i f^{(n-i)}$ to the integral $I_{0,+}^{1-\gamma} f(n\Delta t)$. We approximated $\int_{j\Delta t}^{(j+1)j\Delta t} f(t - t') \frac{t'^{-\gamma}}{\Gamma(1-\gamma)} \, \mathrm{d}t'$ by using $\frac{f^{n-j} + f^{n-j-1}}{2} \int_{j\Delta t}^{(j+1)j\Delta t} \frac{t'^{-\gamma}}{\Gamma(1-\gamma)} \, \mathrm{d}t'$, which yields

$$\frac{\Delta t^{1-\gamma}}{2\Gamma(2-\gamma)} \left[f^{(n)} + \Sigma_{j=1}^{n-1} f^{(n-j)}((j+1)^{1-\gamma} - (j-1)^{1-\gamma}) + f^{(0)}(n^{1-\gamma} - (n-1)^{1-\gamma}) \right]$$

for $I_{0,+}^{1-\gamma} f$. Checking the above discretization of $(\mathrm{Id} + \lambda I_{0,+}^{1-\gamma})^{-1}$ against the Laplace convolution of kernel $\mathcal{H}_{\lambda,\gamma}$ (see appendix C), we found an overall relative error of less than 10^{-2} per cent, with time step $\Delta t = 10^{-3}$. Figure 1 was obtained this way.

4.2. Discretizing (1) and (4)

In order to avoid a strongly restrictive stability condition imposing very small time steps, an implicit scheme for (1) [39] is recommended, with second-order accurate expressions for space derivatives, as in appendix D. Discretizing $(\mathrm{Id} + \lambda I_{0,+}^{1-\gamma})^{-1}$ as above allowed us to solve (4) according to method 1 of appendix D. An alternative way (method 2 of appendix D) consists in discretizing the Caputo derivative in (1). To do this, we used a scheme of the order of $2 - \gamma$ [40] instead of an expression of the order of 1, based upon Grünwald–Letnikov's formula [41] which is known to yield a converging solution to (2).
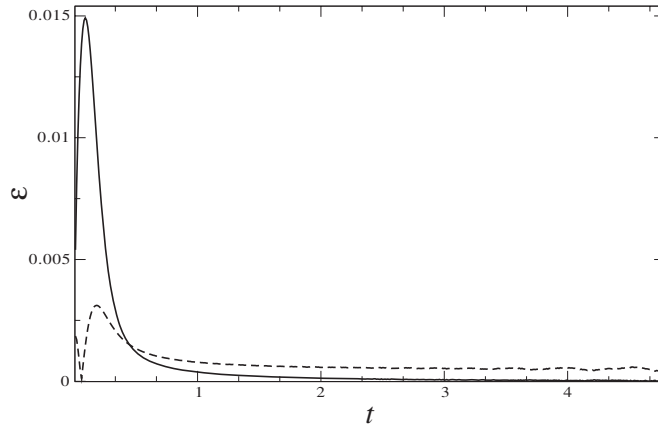
Figure 2. Relative error ε for the numerical solution of (1), with methods 1 and 2, in a particular case where an exact solution is available. Method 1 corresponds to dashed lines, full line stands for method 2, and we have set $\gamma = 3/4$, $\lambda = 1$ and $v = 10$. Space and time steps are $\Delta x = 10^{-2}$ and $\Delta t = 10^{-3}$.

We checked both methods against

$$C(x, t) = \mathcal{A}(t)\, e^{vx/(2K)} \sin \pi x$$

which exactly solves (1) or (4) in]0, 1[, and satisfies $C(0, t) = C(1, t) = 0$, provided $\mathcal{A}(t)$ satisfies the ordinary differential equation

$$\left(\partial_t + \lambda \partial_t^\gamma\right)\mathcal{A}(t) = -\Lambda \mathcal{A}(t)$$

with $\mathcal{A}(0) = 1$ and $\Lambda = \pi^2 K + v^2/(4K)$. Following [28], $\mathcal{A}(t)$ is the inverse Laplace transform of $\frac{1+\lambda s^{\gamma-1}}{s+\lambda s^\gamma + \Lambda}$, equal to

$$\mathcal{A}(t) = \frac{\Lambda \lambda \sin \pi \gamma}{\pi} \int_0^\infty \frac{e^{-\rho t} \rho^{\gamma-1}}{(\Lambda - \rho)^2 + \lambda^2 \rho^{2\gamma} + 2\lambda(\Lambda - \rho)\rho^\gamma \cos(\gamma\pi)}\, d\rho. \qquad (12)$$

Comparisons displayed on figure 2, show that method 1 is slightly more accurate at early times while method 2 is better at late times. For simulations presented in the next subsection we used both, and discrepancies were not visible. Grünwald–Letnikov's scheme yields relative errors of about four times that of methods 1 and 2. Similar checks were performed for fluxes. From the discretized density $C(x, t)$, we derived the flux according to (5) and subsection 4.1. An exact expression for the flux corresponding to the example, used for the above checks is

$$F(x, t) = \left(\text{Id} + \lambda I_{0,+}^{1-\gamma}\right)^{-1} \mathcal{A}(t)\, e^{vx/(2K)} (v \sin(\pi x)/2 - K\pi \cos(\pi x)), \qquad (13)$$

where $\mathcal{A}$ satisfies (12), so that $(\text{Id} + \lambda I_{0,+}^{1-\gamma})^{-1} \mathcal{A}(t)$ has Laplace transform $\frac{1}{s+\lambda s^\gamma + \Lambda}$. Comparing fluxes, numerically computed or given by the exact solution (13) yields issues, very similar to figure 2, with an overall relative error of less than 2%.

4.3. Monte Carlo simulations of density and fluxes for $Y(t)$

In order to represent the density of $Y(t)$, let us consider, as in [15], a discrete time random walk with independent jumps, separated by waiting times of identical duration dt. Jumps (w.r.t. a frame, moving at speed v) distributed as lN, with N a Gaussian random variable as in subsection 3.1, yield a process whose limit is $X(t)$ when time- and length-scales dt
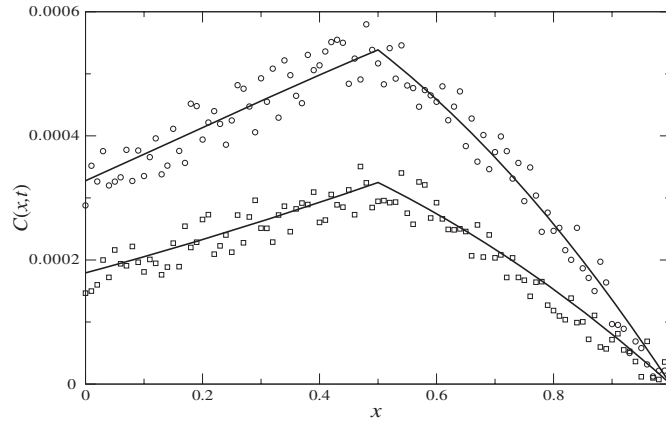
Figure 3. The density of $Y(t)$ according to Monte Carlo simulation and discretization of (1). Circles and squares represent normalized histograms of a random walk as in subsection 3.3, with $Q = 10^4$ walkers, at times $t = 1$ and $t = 2$, respectively. Full line stands for the discretized equation (1). Parameters are $K = 1, \gamma = 1/2, \lambda = 1$ and $v = 1$. Simulations were started (at instant 0) from a uniform distribution, concentrated on a very small interval near $x = 0.5$.

and l tend to zero. If we impose $K = l^2/(2\mathrm{d}t)$, the density of particles tends to $q(x, t)$, which satisfies (8). To approximate p and $Y(t)$, we impose that the jump of rank n takes place at instant $n\mathrm{d}t + W_1 + \cdots + W_n$ (instead of $n\mathrm{d}t$), the W_i being independent random variables distributed as $\Theta S_\gamma(1, 1, 0)$. According to the notations of [14], $S_\gamma(\beta = 1, \sigma = 1, 0)$ denotes a totally skewed, normalized, stable random variable of exponent γ without bias, whose p.d.f. has Laplace transform $\mathrm{e}^{-s^\gamma/\cos(\pi\gamma/2)}$. The random variable $W_1 + \cdots + W_n$ has p.d.f. $n^{1/\gamma}\Theta S_\gamma(1, 1, 0)$ whose Laplace transform is $\mathrm{e}^{-(\Theta s)^\gamma n/\cos(\pi\gamma/2)}$, itself equal to $\mathrm{e}^{-\lambda\tau s^\gamma}$ for $n\,\mathrm{d}t = \tau$, provided we set $\Theta^\gamma = \lambda\,\mathrm{d}t\cos(\pi\gamma/2)$. Histograms represent the density of walkers.

Figure 3 compares histograms against numerical solutions to (1) or (4), starting from a uniform density concentrated on a small sub-interval. The agreement provides a visual proof of the theorem, which states that equations (1)–(4) indeed rule the density of $Y(t)$. Figure 4 shows outlet fluxes issued from both methods, and illustrates (5), which extends Fick's law to heavy-tailed sticking times.

Similar comparisons will help in understanding that (4) is suitable to situations where, instead of being launched together at time $t = 0$, walkers are delivered progressively.

5. A model for advection–dispersion with immobile periods, accounting for sources

In general, at the laboratory or at the field scale, tracer injection may not be instantaneous, and generic source rate $r(x, t)$ must be taken into account.

Of course, simply adding $r(x, t)$ on the right-hand side of (1) or (4) does not yield equivalent problems; this also holds for (2) and (3) [23]. The appropriate equation for advection–dispersion with immobile periods involving sources is

$$\partial_t C(x, t) = L\big(\mathrm{Id} + \lambda I_{0,+}^{1-\gamma}\big)^{-1} C(x, t) + r(x, t), \tag{14}$$

equivalent to

$$\partial_t C(x, t) + \lambda\partial_t^\gamma C(x, t) = LC(x, t) + \big(\mathrm{Id} + \lambda I_{0,+}^{1-\gamma}\big)r(x, t).$$
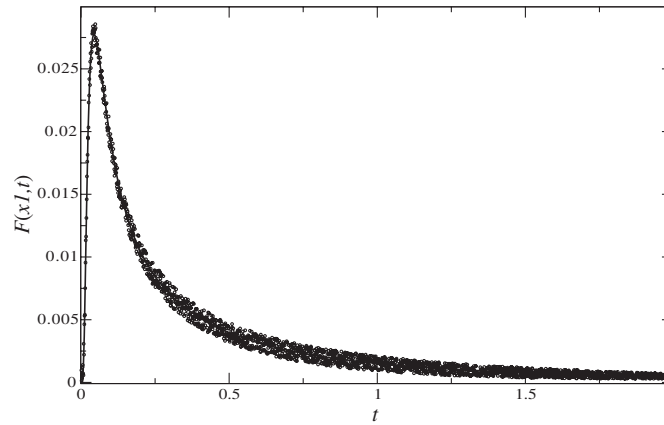
Figure 4. The flux of particles at the absorbing outlet x_1 of domain $]x_0, x_1[$, across time. Circles represent number of walkers crossing the outlet during small time intervals, the flux computed from (1) and (4) corresponds to the full line. Parameters and initial data are as for figure 3.
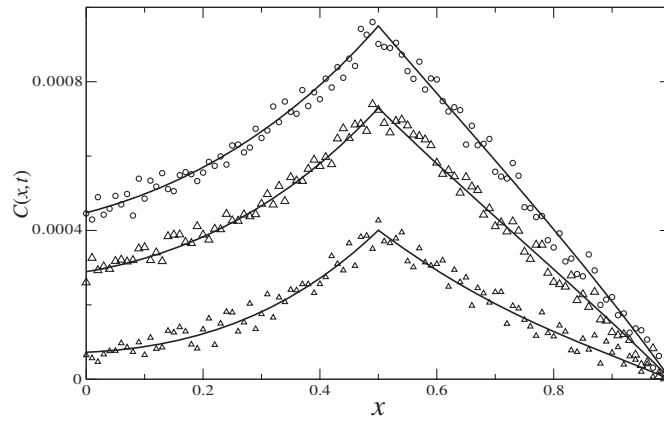

Figure 5. The density of $Y(t)$ according to Monte Carlo simulation and discretization of (14), with $r(x, t)$ constant for $0 \leqslant t \leqslant t_0 = 0.5$. Snapshots, represented at the left, correspond to an active source: upright large and small triangles represent times $t = 0.1$ and $t = 0.3$, respectively. Circles denote time $t = t_0 = 0.5$ when the source was switched off. Snapshots obtained after t_0 are displayed on the right: downward small and large triangles denote $t = 0.7$ and $t = 0.9$, respectively. Time t_0 (circles) has been represented also. Parameters are the same as used for figure 3.

To see this, recall that, according to subsection 3.2, (1) and (4) rule the evolution of the density $C(x, t)$ of a cloud of walkers started from initial density $C(x, 0) = \varphi(x)$, and note that starting the process at time τ (instead of 0) would yield density $C(x, t - \tau)$. In Laplace variables, we easily see that this is equivalent to taking initial data equal to zero, while adding source rate $r(x, t) = \varphi(x)\delta(t - \tau)$ on the right-hand side of (4), which yields a particular case of (14). Hence, with this expression for r, (14) represents the density of a cloud of walkers started from an instantaneous source. We pass to the general case on the basis of the linear character of the problem, since walkers were assumed to be independent. Then, for a source, active for $0 \leqslant t < t_0$ (where t_0 may be finite or not), we just have to add
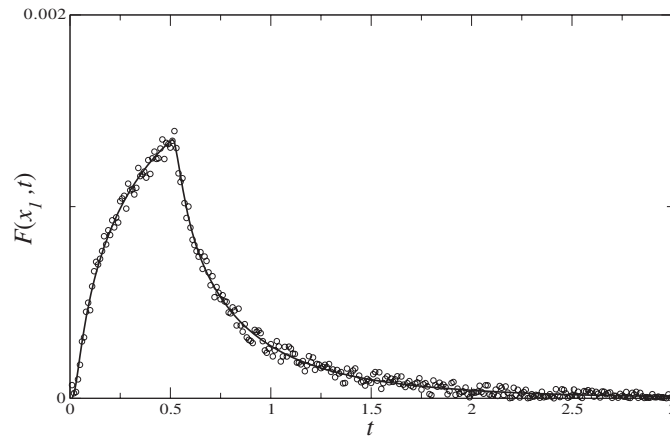
Figure 6. The flux of particles at x_1, across time, when particles are delivered according to rate $r(x, t)$, as for figure 5. Circles represent Monte Carlo simulations, and full line stands for fluxes computed according to (5) after concentration was obtained from (14). Parameters are as for figure 3.

up densities, or equivalently instantaneous sources of the above particular case, according to $r(x, t) = \int_0^{t_0} r(x, \tau)\delta(t - \tau)\,\mathrm{d}\tau$.

Figures 5 and 6 represent a visual proof of this point, with $r(x, t)$ constant in a small interval concentrated near $x = 0.5$, during time interval $[0, 0.5]$. After that the source was switched off.

6. Conclusion

The fractal MIM model was proposed by Zang *et al* [19] and Schumer *et al* [15]. It represents advection–dispersion of particles which can get stuck in immobile traps, and then be released. The trapping times have a random duration, distributed according to a stable Lévy law. This point was proved within the framework of small-scale motions, accumulating independent displacements, normally distributed as for classical diffusion. Here, for each time τ globally spent in motion, the total immobile period is given by a Lévy process $U(\tau)$, stable and taking only positive values, which implies a stability exponent γ between 0 and 1. We proved that the density of particles performing such a random walk, started from initial data at instant $t = 0$, satisfies (1).

Then, the flux of particles is given by Fick's law provided that we apply it to a definite functional of the concentration, which is a non-local-in-time mapping accounting for the memory of the past, and for the release of previously trapped particles. In fact, this functional computes the density of mobile walkers, available for transport (not trapped), and can be defined as the inverse of another (non-local) mapping. It is also equal to a convolution whose kernel involves a function of the Mittag–Leffler type. The time mapping is easily discretized. For computations, we found that inverting the non-local mapping is more viable and rapid than addressing the convolution. Nevertheless, results of [45] may help us using the convolution. At early times, the mapping giving the density of mobile walkers almost coincides with identity, and fluxes accounting for immobilizations are almost Fickian, since few particles are trapped. At late times, instead, the mapping is approximately proportional to the Riemann–Liouville derivative of the order of $1 - \gamma$, as when the fractional Fokker–Planck equation holds.

The obtained expression for fluxes allowed us to identify in the fractal MIM model a conservation law (4), which appears to be more suitable than (1) to account for particles that are injected progressively, as frequently happens in transport experiments. Sources can easily be incorporated on the right-hand side of (4), which yields the inhomogeneous form of the fractal MIM model (14); the forcing r represents a source rate, possibly distributed in time and space. It now remains to prove that (4) and (14) still represent advection–dispersion with heavy-tailed immobile periods when parameters such as K and v depend on time.

The reasoning would adapt to slightly more general macroscopic models with a fractional Riesz–Feller derivative of order α between 1 and 2 instead of the usual second-order derivative which we considered in (1) and (4) [46, 47]. We then would have a space derivative of the order of $\alpha - 1$ in place of Fickian diffusive flux in (5), and some care would be necessary to handle boundary conditions [36]. But the time mapping computing the concentration of mobile particles would be exactly the same. Passing to 'shorter' sticking times, oppositely [24, 42], with larger values of γ, would not consist in a straightforward generalization of the reasoning, presented here, and many important steps would need being deeply revisited.

Acknowledgments

Appendix A. Definition of fractional integrals and derivatives

Fractional integral and derivatives generalize to non-integer orders the repeated integrals and derivatives [27–31] according to the following definitions.

Definition 1. *When α is positive, the fractional integral of the order of α is*

$$I_{0,+}^{\alpha} f(t) = \frac{1}{\Gamma(\alpha)} \int_0^t (t - t')^{\alpha-1} f(t') \, dt'.$$

In equations (1) and (2), we use the Caputo derivative, and an other mapping, called Riemann–Liouville derivative, appears in (3).

Definition 2. *The Caputo fractional derivative $\partial_t^{\alpha} f$ of function f, of the order of α strictly between integers n and $n + 1$, is $\partial_t^{\alpha} f(t) = I_{0,+}^{n+1-\alpha} \partial_t^{n+1} f(t)$.*

Definition 3. *The Riemann–Liouville fractional derivative $D_{0,+}^{\alpha} f$ of the order of α, on $[0, t]$ is $D_{0,+}^{\alpha} f(t) = \partial_t^{n+1} I_{0,+}^{n+1-\alpha} f(t)$.*

The difference between both derivatives is [28]

$$D_{0,+}^{\alpha} f(t) - \partial_t^{\alpha} f(t) = \Sigma_{k=0}^{n} \frac{t^{k-\alpha}}{\Gamma(k + 1 - \alpha)} \partial_t^k f(0+).$$

Using Laplace variables, and setting $\mathcal{L}(f)(s) = \tilde{f}(s) = \int_0^{+\infty} e^{-st} f(t) \, dt$ for the Laplace transform of function f, yields useful formulae for fractional calculus, according to the following remark.

Remark 1. In Laplace variables we have

$$\mathcal{L}\big(I_{0,+}^{\alpha} f\big)(s) = s^{-\alpha} \tilde{f}(s),$$
$$\mathcal{L}\big(\partial_t^{\alpha} f\big)(s) = s^{\alpha} \tilde{f}(s) - \Sigma_{k=0}^{n} \partial_t^k f(0+) s^{\alpha-1-k},$$

and

$$\mathcal{L}\big(D_{0,+}^{\alpha} f\big)(s) = s^{\alpha}\tilde{f}(s) - \Sigma_{k=0}^{n}\partial_{t}^{k} I_{0,+}^{n+1-\alpha} f(0+)s^{n-k},$$

for α between integers n and $n + 1$.

Appendix B. Inverting $\big(\mathrm{Id} + \lambda I_{0,+}^{1-\gamma}\big)$ and more general similar mappings

The inverse makes sense in $L^{p}[0, T]$ due to Neumann series when T is small. Indeed, when functions g and h belong to $L^{p}[0, T]$ and $L^{1}[0, T]$, the convolution $g * h(t) = \int_{0}^{t} g(t - t')h(t')\,\mathrm{d}t'$ satisfies Young's inequality [30]

$$\|g * h\|_{L^{p}[0,T]} \leqslant \|g\|_{L^{p}[0,T]}\|h\|_{L^{1}[0,T]}.$$

Taking $h(t) = t^{\alpha-1}/\Gamma(\alpha)$ we obtain $\|I_{0,+}^{\alpha} f\|_{L^{p}[0,T]} \leqslant \|f\|_{L^{p}[0,T]}\frac{T^{\alpha}}{\Gamma(\alpha+1)}$, so that the mapping $I_{0,+}^{\alpha}$ is bounded in the Banach space $L^{p}[0, T]$. Hence, the series $\Sigma_{n\geqslant 0}\big(-\lambda I_{0,+}^{1-\gamma}\big)^{n}$ inverts $\mathrm{Id} + \lambda I_{0,+}^{1-\gamma}$ in $L^{p}[0, T]$, provided T satisfies $\lambda T^{\alpha} < \Gamma(\alpha + 1)$.

We will see that $\big(\mathrm{Id} + \lambda I_{0,+}^{1-\gamma}\big)^{-1}$ exists at all times. In fact, $\big(\mathrm{Id} + \lambda I_{0,+}^{1-\gamma}\big)$ is a particular case of $\mathrm{Id} + \int_{0}^{1} \bar{w}(\mathrm{d}\beta)I_{0,+}^{\beta_{\max}-\beta}$, and we will prove the following proposition.

Proposition 1. *Let $\bar{w}$ be a finite measure, concentrated on $[0, \beta_{\max}] \subset [0, 1]$, and satisfying*

$$\int_{0}^{\beta_{\max}} \chi^{\beta-\beta_{\max}}|\bar{w}(\mathrm{d}\beta)| < 1 \tag{B.1}$$

with χ in R^{+}. Then, $\mathrm{Id}+\int_{0}^{1} \bar{w}(\mathrm{d}\beta)I_{0,+}^{\beta_{\max}-\beta}$ is invertible, with inverse $\Sigma_{n\geqslant 0}\big(-\int_{0}^{1} \bar{w}(\mathrm{d}\beta)I_{0,+}^{\beta_{\max}-\beta}\big)^{n}$ in the Banach space $X_{\chi} = \{f/\|e_{-\chi} f\|_{L^{p}[0,T]} < \infty\}$, with weight $e_{-\chi}(t) = \mathrm{e}^{-\chi t}$.

Proof. The lemma 3 of [43] states that $\big\|e_{-\chi} I_{0,+}^{\alpha} f\big\|_{L^{p}[0,T]} \leqslant \chi^{-\alpha}\|e_{-\chi} f\|_{L^{p}[0,T]}$ for every f in X_{χ}. This implies

$$\left\|e_{-\chi}\int_{0}^{\beta_{\max}} \bar{w}(\mathrm{d}\beta)I_{0,+}^{\beta_{\max}-\beta} f\right\|_{L^{p}[0,T]} \leqslant \int_{0}^{\beta_{\max}} \chi^{\beta-\beta_{\max}}|\bar{w}(\mathrm{d}\beta)|\|e_{-\chi} f\|_{L^{p}[0,T]},$$

hence the mapping $\int_{0}^{\beta_{\max}} \bar{w}(\mathrm{d}\beta)I_{0,+}^{\beta_{\max}-\beta}$ is bounded by $\int_{0}^{\beta_{\max}} \chi^{\beta-\beta_{\max}}|\bar{w}(\mathrm{d}\beta)|$ in X_{χ}, so that the Neumann series $\Sigma_{n\geqslant 0}\big(-\int_{0}^{1} \bar{w}(\mathrm{d}\beta)I_{0,+}^{\beta_{\max}-\beta}\big)^{n}$ converges in this space, with sum $\big(\mathrm{Id} + \int_{0}^{1} \bar{w}(\mathrm{d}\beta)I_{0,+}^{\beta_{\max}-\beta}\big)^{-1}$, due to (B.1). $\qquad\square$

Remark 2. With $\beta_{\max} = 1$ and $\bar{w} = \lambda\delta_{\gamma}$, we have $\int_{0}^{1} \bar{w}(\mathrm{d}\beta)I_{0,+}^{\beta_{\max}-\beta} = \lambda I_{0,+}^{1-\gamma}$, and the Proposition 1 states that $\big(\mathrm{Id} + \lambda I_{0,+}^{1-\gamma}\big)^{-1}$ exists in X_{χ} provided we take χ such that $0 < \lambda\chi^{\gamma-1} < 1$.

More generally, the above proposition implies that wit $w = \bar{w} + \delta_{\beta_{max}}$, the mapping

$$\int_{0}^{1} w(\mathrm{d}\beta)I_{0,+}^{1-\beta} = I_{0,+}^{1-\beta_{\max}}\left(\mathrm{Id} + \int_{0}^{\beta_{max}} \bar{w}(\mathrm{d}\beta)I_{0,+}^{\beta_{\max}-\beta}\right)$$

has a left inverse, which is $\big(\mathrm{Id} + \int_{0}^{\beta_{\max}} \bar{w}(\mathrm{d}\beta)I_{0,+}^{\beta_{\max}-\beta}\big)^{-1} D_{0,+}^{1-\beta_{\max}}$. For $\beta_{\max} = 1$, it even is a true inverse. Hence, for particles spreading according to $\int_{0}^{1} w(\mathrm{d}\beta)\partial_{t}^{\beta} C = LC$, the flux is $(-K\nabla + v)\big(\mathrm{Id} + \int_{0}^{\beta_{\max}} \bar{w}(\mathrm{d}\beta)I_{0,+}^{\beta_{\max}-\beta}\big)^{-1} D_{0,+}^{1-\beta_{\max}}$.

14

Appendix C. The mapping $\left(\mathrm{Id} + \lambda I_{0,+}^{1-\gamma}\right)^{-1}$ when t is large

In Laplace variables, the mapping $\left(\mathrm{Id} + \lambda I_{0,+}^{1-\gamma}\right)^{-1}$ has symbol $\frac{s^{1-\gamma}}{s^{1-\gamma}+\lambda}$, according to the remark of appendix A. The symbol is the Laplace transform of function $\mathcal{H}_{\lambda,\gamma}$ defined below, using the Mittag–Leffler type function $E_\alpha(z) = \Sigma_{n \geqslant 0} \frac{z^n}{\Gamma(1+n\alpha)}$ described in [28].

Notation: For positive valued t and λ and with γ between 0 and 1, let us set $\mathcal{H}_{\lambda,\gamma}(t) = \frac{\mathrm{d}}{\mathrm{d}t} E_{1-\gamma}(-\lambda t^{1-\gamma})$.

The mapping $\left(\mathrm{Id} + \lambda I_{0,+}^{1-\gamma}\right)^{-1}$ is equal to the convolution of kernel $\mathcal{H}_{\lambda,\gamma}$, which satisfies $\mathcal{H}_{\lambda,\gamma}(t) = \Sigma_{n=0}^{\infty} \frac{-\lambda t^{1-\gamma}}{\Gamma(1+n(1-\gamma))}$ for $t > 0$, and belongs to $L^{p'}(R^+)$ for $p' > 1$. From this, we will deduce that $\left(\mathrm{Id} + \lambda I_{0,+}^{1-\gamma}\right)^{-1} f(t)$ and the Riemann–Liouville derivative $D_{0,+}^{1-\gamma} f(t)$ of f become very similar when t tends to infinity, according to the following proposition.

Proposition 2. *For any function f belonging to $L^p(R^+)$, provided the Riemann–Liouville derivative $D_{0,+}^{1-\gamma} f = \varphi$ exists in $L^p(R^+)$, expression $\left[\left(\mathrm{Id} + \lambda I_{0,+}^{1-\gamma}\right)^{-1} - \lambda^{-1} D_{0,+}^{1-\gamma}\right] f(t)$ tends to zero when t tends to infinity.*

Proof. We have $f = I_{0,+}^{1-\gamma} \varphi$, with φ in $L^p(R^+)$ ([30, 31]), and

$$\left[\left(\mathrm{Id} + \lambda I_{0,+}^{1-\gamma}\right)^{-1} - \lambda^{-1} D_{0,+}^{1-\gamma}\right] f(t) = -\lambda^{-1}\left(\mathrm{Id} + \lambda I_{0,+}^{1-\gamma}\right)^{-1} \varphi(t).$$

To see that the latter expression, proportional to $\mathcal{H}_{\lambda,\gamma} * \varphi(t)$, tends to zero when t tends to infinity, let us take p' such that $1/p' + 1/p = 1$. We have

$$|\varphi * \mathcal{H}(t)| \leqslant \left| \int_0^{t-A} \varphi(t-x)\mathcal{H}(x)\,\mathrm{d}x \right| + \left| \int_{t-A}^{\infty} \varphi(t-x)\mathcal{H}(x)\,\mathrm{d}x \right|$$

$$\leqslant \|\mathcal{H}\|_{L^{p'}} \left(\int_A^{t-A} |\varphi(y)|^p\,\mathrm{d}y \right)^{1/p} + \|\varphi\|_{L^p} \left(\int_A^{\infty} |\mathcal{H}(y)|^{p'}\,\mathrm{d}y \right)^{1/p'}$$

for $A < t$. For any given $\varepsilon > 0$, the latter integrals will be less than $\varepsilon/2$ if we take A large enough to ensure $\int_A^{\infty} |\varphi(y)|^p\,\mathrm{d}y \|\mathcal{H}\|_{L^{p'}}^p < (\varepsilon/2)^p$ and $\int_A^{\infty} |\mathcal{H}(y)|^{p'}\,\mathrm{d}y \|\varphi\|_{L^p}^{p'} < (\varepsilon/2)^{p'}$. Such a A exists, because $\mathcal{H}$ and φ belong to $L^p(R^+)$. $\qquad\square$

Appendix D. Two implicit schemes for (1) and (4)

For space derivatives $\partial_{x^2}^2 C(i\Delta x, n\Delta t)$ and $\partial_x C(i\delta x, n\Delta t)$ in (1) or (4), not surprisingly we take second-order schemes $\Delta x^{-2}\left[C_{i+1}^{(n)} - 2C_i^{(n)} + C_{i-1}^{(n)}\right]$ and $(2\Delta x)^{-1}\left[C_{i+1}^{(n)} - C_{i-1}^{(n)}\right]$.

A simple trapezoidal integration rule yields $\Sigma_{j=0}^n w_j C_i^{n-j}$ (method 1) for $I_{0,+}^{1-\gamma} C(i\Delta x, n\Delta t)$ in (4), and results in the implicit scheme

$$C_i^{(n+1)} - b_0^{(n)}\left[\frac{K\Delta t}{\Delta x^2}\left(C_{i+1}^{(n+1)} - 2C_i^{(n+1)} + C_{i-1}^{(n+1)}\right) - \frac{v\Delta t}{2\Delta x}\left(C_{i+1}^{(n+1)} - C_{i-1}^{(n+1)}\right) \right]$$

$$= C_i^{(n)} + \Sigma_{j=1}^{n+1}\left[b_j^{(n)} \frac{K\Delta t}{\Delta x^2}\left(C_{(i+1)}^{n+1-j} - 2C_i^{(n+1-j)} + C_{i-1}^{(n+1-j)}\right) - \frac{v\Delta t}{2\Delta x}\left(C_{i+1}^{(n+1-j)} - C_{i-1}^{(n+1)}\right) \right]$$

in the interior of the domain. The $b_i^{(n)}$ are easily computed at each time step according to subsection 4.1.

We compared against the scheme obtained from (1) by discretizing the Caputo derivative (method 2). Using for $\partial_t^\gamma C(i\,\Delta x, n\,\Delta t)$ algorithm 1 of [40] yields

$$\left(1 + \frac{\lambda \Delta t^{1-\gamma}}{\Gamma(2-\gamma)}\right) C_i^{(n+1)} - \frac{K\,\Delta t}{\Delta x^2}\left(C_{i+1}^{(n+1)} - 2C_i^{(n+1)} + C_{i-1}^{(n+1)}\right) + \frac{v\,\Delta t}{2\Delta x}\left(C_{i+1}^{(n+1)} - C_{i-1}^{(n+1)}\right)$$

$$= -\frac{\lambda \Delta t^{1-\gamma}}{\Gamma(2-\gamma)}\Sigma_{j=1}^{n+1} a_{j,n}\left(C_i^{(n+1-j)} - C_i^{(0)}\right) + \frac{\lambda \Delta t^{1-\gamma}}{\Gamma(2-\gamma)} C_i^{(0)}$$

where $a_{j,n}$ satisfy $a_{0,n} = 1$, $a_{j,n} = (n+1)^{1-\gamma} - 2n^{1-\gamma} + (n-1)^{1-\gamma}$ for $0 < j < n$ and $a_{n,n} = (1-\gamma)n^{1-\gamma} - n^{1-\gamma} + (n-1)^{1-\gamma}$.

Both methods need solving systems of the form of $MU^{(n+1)} = M'U^{(n)}$, with M a tridiagonal array, and $U^{(n)} = \left(C_0^{(n)}, \ldots C_i^{(n)}, \ldots, C_{\text{imax}}^{(n)}\right)^\dagger$.

References

[1] Scher H and Lax M 1973 *Phys. Rev.* B **7** 4491
[2] Scher H and Lax M 1973 *Phys. Rev.* B **7** 44502
[3] Mainardi F, Luchko Y and Pagnini G 2001 *Fract. Calc. Appl. Anal.* **4** 153
[4] Metzler R and Klafter J 2004 *J. Phys. A: Math. Gen.* **37** R161–208
[5] Scalas E, Gorenflo R and Mainardi F 2004 *Phys. Rev.* E **69** 011107
[6] Zhang Y, Benson D A, Meerschaert M M and Scheffler H P 2006 *J. Stat. Phys.* **123**
[7] Lutsko J F and Boon J P 2008 *Phys. Rev.* E **77** 051103
[8] Einstein E 1956 *Investigations on the Theory of Brownian Movement* (New York: Dover)
[9] Metzler R and Klafter J 2000 *Phys. Rep.* **339** 1
[10] Meerschaert M M and Scheffler H P 2004 *J. Appl. Probab.* **41** 623
[11] Feller W 1970 *An Introduction to Probability Theory and its Applications* (*Wiley series in probability and mathematical statistics* vol II) (New York: Wiley)
[12] Gnedenko B V and Kolmogorov A N 1968 *Limit Distributions for Sums of Independent Variables* (Reading, MA: Addison Wesley)
[13] Lévy P 1937 *Théorie de l'addition des Variables aléatoires* (Paris: Gauthier-Villars)
[14] Meerschaert M M and Scheffler H P 2000 *Limit Distributions for Sums of Independent Random Vectors, Heavy Tails in Theory and Practice* (New York: Wiley)
[15] Zhang Y, Benson D A and Bauemer B 2008 *Water Resour. Res.* **44** W05404
[16] Bromly M and Hinz C 2004 *Water Resour. Res.* **40** W0740
[17] Cortis A, Chen Y, Scher H and Berkowitz B 2004 *Phys. Rev.* E **70** 041108
[18] Jacobs A 2007 Transport bacterien en milieu poreux, Modélisation et application aux cas d'épandage d'effluents *PhD Thesis* University of Avignon
[19] Schumer R, Benson D A, Meerschaert M M and Bauemer B 2003 *Water Resour. Res.* **39** 1296
[20] Van Genuchten M T and Wierenga P J 1976 *Soil. Sci. Soc. Am. J.* **33** 473
[21] Zaslavsky G 1994 *Phys. D* **76** 110
[22] Magdziarz M, Weron A and Weron K 2007 *Phys. Rev* E **75** 016708
[23] Bauemer B, Kurita S and Meerschaert M M 2006 *Fract. Calc. Appl. Anal.* **8** 27
[24] Levy M and Berkowitz B 2003 *J. Contam. Hydrol.* **64** 203
[25] Tufenkji N and Elimelech M 2005 *Environ. Sci. Technol.* **39** 3620–9
[26] Zhang Y, Bauemer B and Benson D A 2006 *Geophys. Res. Lett.* **33** L18407
[27] Butzer P L and Westphal U 2000 *Applications of Fractional Calculus in Physics* ed R Hilfer (Singapore: World Scientific)
[28] Gorenflo R and Mainardi F 1997 *Fractals and Fractional Calculus in Continuum Mechanics* (*CISM courses and lectures* vol 378) ed A Carpinteri and F Mainardi (New York: Springer)
[29] Kilbas A A, Srivastava H M and Trujillo J J 2006 *Theory and Applications of Fractional Differential Equations* (*North-Holland Mathematical Studies* vol 204) ed J Mill (Amsterdam: North-Holland)
[30] Rubin B 1996 *Fractional Integrals and Potentials* (Harlow: Longman)
[31] Samko S G, Kilbas A A and Marichev O I 1993 *Fractional Integrals and Derivatives: Theory and Applications* (New York: Gordon and Breach)
[32] Caputo M 2001 *Frac. Calc. Appl. Anal.* **4** 421
[33] Chechkin A V, Gorenflo R and Sokolov I M 2002 *Phys. Rev.* E **66** 046129

[34] Heinsalu E, Patriarca M, Goychuk I and Hänggi P 2007 *Phys. Rev. Lett.* **99** 120602
[35] Paradisi P, Cesari R, Mainardi F and Tampieri F 2001 *Physica* A **293** 130
[36] Néel M C, Abdennadher A and Joelson M 2007 *J. Phys. A: Math. Theor.* **40** 82999
[37] Gorenflo R, Mainardi F and Vivoli A 2007 *Chaos Soliton Fractal* **34** 87
[38] Piryatinska A, Saichev A I and Woyczynski W A 2005 *Physica* A **349** 375
[39] Langlands T A M and Henry B I 2005 *J. Comput. Phys.* **205** 719
[40] Diethelm K, Ford N J, Freed A D and Luchko Y 2005 *Comput. Methods Appl. Mech. Eng.* **194** 543
[41] Gorenflo R and Abdel-Rehim E A 2007 *J. Comput. Appl. Math.* **205** 871
[42] Meerschaert M M and Scheffler H P 2004 *J. Appl. Probab.* **41** 455
[43] Gorenflo R, Iskenderov A and Yamamoto R 1997 On the regularization of linear Abel-type integral equations
        of first kind with Hölder-continuous kernels preprint available on http://www.math.fu-berlin.de
[44] Gorenflo R and Mainardi F 1999 *Fract. Calc. Appl. Anal.* **1** 167
[45] Fulger D, Scalas E and Germano G 2008 *Phys. Rev.* E **77** 621122
[46] Krepysheva N, Di Pietro L and Néel M C 2006 *Physica* A **368** 335
[47] Zoia A and Kardar Rosso 2007 *Phys. Rev.* E **77** 041115